Brookite-TiO_2-Supported Pt Bilayers for the Low-Temperature Water–Gas Shift Reaction

Wenning Zhao,[#] Junjun Wang,[#] Xixiong Zhang,[#] Guanghui Zhang, Yong Li,[*] Zheng Jiang, Mingrun Li, Yan Zhou, Yuemin Wang,[*] and Wenjie Shen[*]

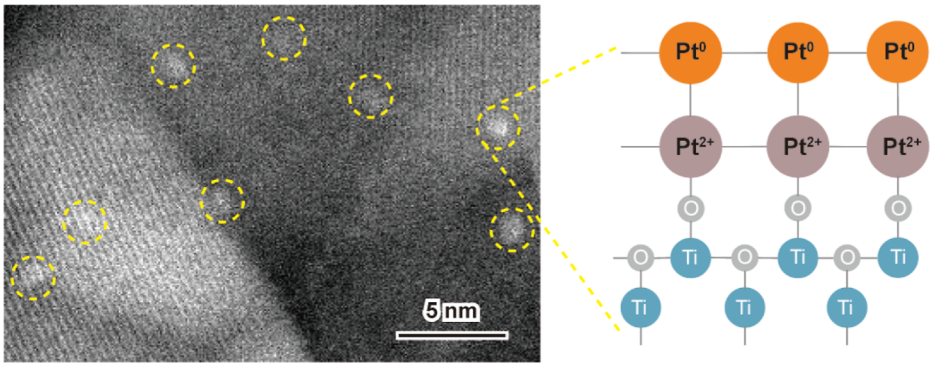

ABSTRACT: Highly dispersed Pt species, typically subnanometric clusters and single-atoms, feature catalysis that differed significantly from that of the faceted nanoparticles. However, the catalytic chemistry of these size-specified Pt entities is still a subject of debate. Here, we report that metallic Pt clusters in a bilayer geometry, dispersed on TiO_2, served as the active phase for the low-temperature water–gas shift reaction. The control of Pt dispersion was done by treating a Pt/TiO_2 sample, where 3 nm Pt particles dispersed over rod-shaped brookite-TiO_2, with oxidative and reductive gases at elevated temperatures (673–873 K). The oxidative treatment of the Pt/TiO_2 precursor yielded subnanometric PtO_x clusters (<1 nm) at 773 K and cationic Pt single-atoms at 873 K. Combined microscopic and spectroscopic characterizations revealed that the PtO_x clusters had a monolayer geometry, in which the Pt atoms were loosely connected via the Pt–O–Pt bond and chemically anchored on the surface of TiO_2 via the Pt–O–Ti bond. While the cationic Pt single-atoms not only located on the surface but also diffused into the subsurface/bulk of TiO_2, presenting in diverse coordination environments. Catalytic evaluations found that the subnanometric PtO_x clusters were more active for the low-temperature water–gas shift reaction than the cationic Pt single-atoms. More interestingly, the H_2-reduction of the PtO_x clusters at 773 K resulted in metallic Pt clusters that adopted predominately a bilayer geometry at an appropriate $Pt^0/(Pt^0 + Pt^{2+})$ ratio. The surficial metallic Pt atoms tuned the electronic structure of the positively charged Pt atoms at the Pt–TiO_2 interface and thus enhanced the catalytic activity dramatically.

KEYWORDS: *Pt/TiO_2 catalyst, Pt bilayer, metal–support interface, active site, low-temperature water–gas shift reaction*

1. INTRODUCTION

The identification of active sites over precious-metal catalysts constitutes the core issue for elaborating the structure-performance relationships. Pt entities, dispersed over reducible oxides, are highly active for producing chemicals in industrial processes and abating exhaust gases from vehicle emissions.[1−4] They are typically present as faceted nanoparticles (2–5 nm), clusters smaller than 2 nm, and single-atoms. Lowering the size of the Pt entities, as small as possible, has been actively pursued to maximize the use of Pt atoms for catalysis. Cumulative experimental data have demonstrated that Pt clusters and single-atoms feature catalysis with exponentially enhanced activity, relative to the faceted nanoparticles.[1,4−7] The chemical nature behind these distinctive performances has been interpreted regarding the size-induced variations in the geometric and electronic structures of the smaller Pt entities.[1,8,9]

However, the increase in catalytic activity is not always straightforward with a decrease in the size of Pt entities from nanoparticles to clusters and ultimately single-atoms. With this regard, Pt/TiO_2 sets a typical example for the low-temperature

water−gas shift (WGS) reaction, where the catalytic activity is commonly associated with the geometric and electronic structure of the Pt−TiO_2 interface.[10−12] The interfacial Pt atom adsorbed CO and the neighboring oxygen vacancy on TiO_2 activates H_2O. For Pt clusters, the interfacial Pt atoms are usually positively charged via strong bonding with TiO_2 for keeping the smaller size, while their electronic structure is further tuned sensitively by the surficial metal atoms, which affects the activity. Pt entities in the size range of 1.2−16.2 nm, dispersed on TiO_2, showed similar turnover frequencies (TOFs) and activation energies (65.6−71.5 kJ mol^{-1}) for the low-temperature WGS reaction.[13] The TOFs, in terms of surface Pt atoms, kept consistent, irrespective of Pt sizes in a range of 0.7−5.0 nm on TiO_2.[14] By contrast, the TOF increased by about 11 times as the Pt size decreased from 2.6 to 1.0 nm over TiO_2.[15] This was ascribed to the higher fraction of $Pt^{\delta+}$ on the smaller clusters, which weakly adsorbed CO. In the case of Pt single-atoms on TiO_2, the cationic nature of Pt atoms and their bonding strength to CO, either weaker[16] or stronger,[17] was invoked to explain the different and even opposite observations on the WGS activities. For instance, a comparative study on Pt entities over TiO_2 concluded that the cationic Pt single-atoms strongly bonded with CO and thus inhibited proceeding of the WGS reaction, whereas Pt particles adsorbed CO only moderately such that it readily reacted with H_2O.[17] Pt clusters (1.6 nm) and cationic single-atoms, dispersed on TiO_2, had similar activation energies in the WGS reaction, but the specific reaction rate (Pt-mass based) on the single-atoms doubled relative to that on the clusters.[18] Spectroscopic characterizations suggested that the cationic Pt single-atom presented as a Pt(II)−$O(OH)_x$− species acted as the active sites. All these reports indicated that the WGS activities of Pt entities experienced a drastically change beyond a threshold size due to the variations in the electronic and geometric structure of the exposed metal atoms,[1,19] which altered the adsorption and activation of the reacting molecules, typically CO. However, a quantitative description for the working mechanism from nanoparticles to clusters and to single-atoms remains challenging, primarily because of the difficulty in precisely controlling the size and finely tuning the chemical state of Pt entities in the catalyst system.

In this work, we investigated the catalytic chemistry of Pt clusters and single-atoms for the low-temperature WGS reaction and further differentiated the catalytic character of oxidized and metallic Pt clusters. It was found that the catalyst containing subnanometric PtO_x clusters was much more active than the catalyst consisting of cationic Pt single-atoms that mostly diffused into the subsurface/bulk of the TiO_2 support. H_2-reduction of the PtO_x clusters at 773 K led to the formation of metallic Pt clusters at similar size but in a bilayer geometry. The surficial metallic Pt atoms tuned the electronic feature of the interfacial positively charged Pt atoms for CO adsorption and activation and thereby prompted the WGS activity significantly.

2. EXPERIMENTAL SECTION

2.1. Catalyst Preparation. The rod-shaped brookite-TiO_2 support was synthesized by a hydrothermal method. One mL of tetrabutyl titanate [$Ti(OBu)_4$] was added dropwise into a solution containing 1 g of NaF, 2 mL of water, and 75 mL of ethanol. The mixture was stirred at room temperature for 30 min and transferred into a 100 mL Teflon-lined autoclave. It was then heated to 473 K and kept at that temperature for 24 h. After cooling down to room temperature, the precipitate was collected by filtration, washed with water and ethanol, dried at 353 K for 12 h in vacuum, and finally calcined at 773 K for 4 h in air.

Pt colloids with a mean size of 2.9 nm were prepared by refluxing a mixture of $H_2PtCl_6{\cdot}6H_2O$ (125 μmol), polyvinylpyrrolidone (PVP, 133 mg), 20 mL of water, and 180 mL of methanol at 353 K for 3 h. The product was collected by evaporating water and methanol, thoroughly washed with water and acetone, and dispersed in 50 mL of water, giving a Pt colloid concentration of 4.5 mol/L.

The initial Pt/TiO_2 sample was prepared by a colloid-deposition method. 0.1 g of TiO_2 was dispersed in 50 mL of ethanol and sonicated for 30 min at room temperature. 0.42 mL of Pt colloid aqueous solution (4.5 mol/L) was diluted with 25 mL of ethanol, gradually dropped into the TiO_2 slurry, and stirred for 4 h. The precipitate was collected by centrifugation, washed with water, and dried at 353 K for 12 h, yielding the Pt/TiO_2 sample.

The dispersion of Pt particles into clusters and single-atoms was done by calcining the Pt/TiO_2 sample in air. Specially, air-calcination of the Pt/TiO_2 sample at 773 K for 4 h decomposed the Pt particle into PtO_x clusters less than 1 nm, labeled as Pt−C. For obtaining the atomically dispersed Pt sites, referring to Pt−A, the Pt/TiO_2 sample was subjected to a two-step calcination process, first at 773 K for 24 h and then at 873 K for 10 h. Pt loadings in these samples were around 0.19 wt %, as determined using inductively coupled plasma atomic emission spectroscopy over a Plasma-Spec-II spectrometer.

2.2. Catalyst Characterization. Nitrogen adsorption−desorption isotherms were recorded at 77 K using an ASAP 2000 instrument (Micromeritics). Before the measurement, the sample was degassed at 573 K for 3 h. The surface area was calculated by a multipoint Brunauer−Emmett−Teller analysis of the adsorption isotherm. Surface areas of the Pt−C and Pt−A samples were 64 and 44 m^2/g, respectively.

Transmission electron microscopy (TEM) images were taken over a JEOL F200 microscope operated at 200 kV. Aberration-corrected high-angle annular dark-field scanning transmission electron microscopy images were acquired using a JEOL-ARM 300F microscope operated at 300 kV. The specimen was prepared by ultrasonically dispersing the powder sample in ethanol, depositing droplets of the suspensions onto lacey carbon-coated copper grids, and drying in air.

X-ray photoelectron spectra (XPS) were recorded on an ESCALAB 250Xi spectrometer (Thermo Fisher Scientific) using an Al Kα radiation source. The sample was pressed into a thin disc and mounted onto the sample holder that was placed in the analysis chamber. For the H_2-reduced sample, the as-calcined sample was sequentially reduced with H_2 in the pretreatment chamber at 473, 573, and 773 K for 2 h and then transferred into the analysis chamber, where the spectra of Ti 2p, Pt 4f, and O 1s were recorded. The charging effect was corrected by adjusting the binding energy of C 1s to 284.6 eV. Deconvolution of the spectra was done by subtracting the Ti 3s energy loss XPS feature from Pt $4f_{5/2}$ at 75.0 eV.

X-ray absorption near-edge structure (XANES) and extended X-ray absorption fine structure (EXAFS) spectra of Pt K-edges were measured at the BL14W1 beamline at the Shanghai Synchrotron Radiation Facility, China. The X-ray was monochromatized by a double-crystal Si(311) monochromator. The storage ring was operated at 3.5 GeV with a current of 230 mA. The sample was pressed into a self-

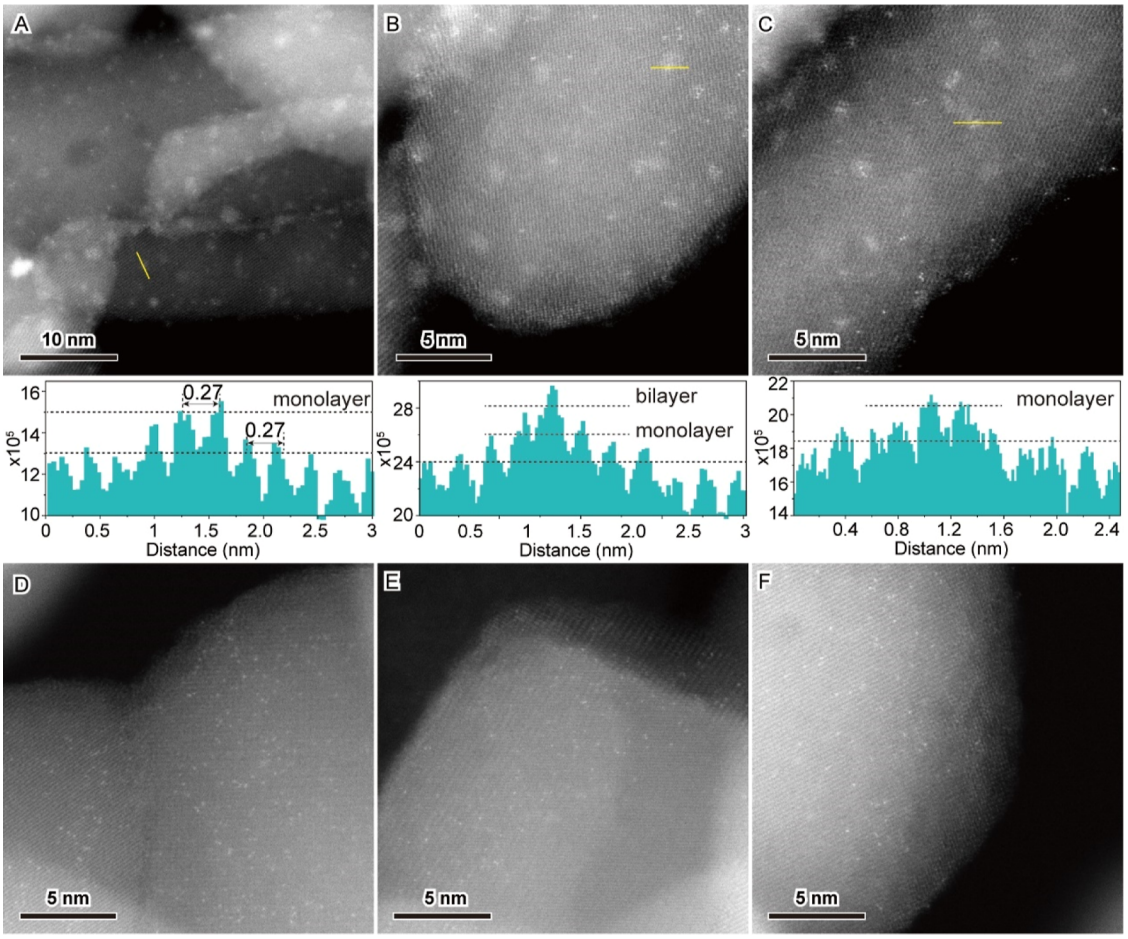

Figure 1. STEM images of the Pt−C (A−C) and Pt−A (D−F) samples. The line intensity profiles correspond to the marked regions on the STEM images.

supporting wafer and mounted into a reaction cell, where the spectra were recorded at room temperature. EXAFS data were processed according to the standard procedures using the Athena and Artemis modules of the IFEFFIT software packages. EXAFS contributions were separated from different coordination shells by using hanning windows (dk = 1.0 $Å^{-1}$). Quantitative curve-fittings were carried out in the *R*-space (Pt 1.2−3.7 Å) with a Fourier transform *k*-space range (Pt 3.2−11.5 $Å^{-1}$). The overall amplitude reduction factor, S_0^2, was set to 0.82 for the Pt K-edge, obtained by fitting the reference Pt foil.

Infrared (IR) spectra of CO adsorption were recorded on an ultrahigh vacuum (UHV) apparatus, combing an IR spectrometer (Bruker Vertex 80v) and a multichamber UHV system (Prevac). 200 mg of sample was pressed into an inert metal mesh and mounted on a sample holder that was specially designed for the transmission model operation. The sample was vacuumed at 373 K and treated with atomic hydrogen at the desired temperature (473−773 K) for 1 h. Exposure to CO was achieved by using a leak-valve-based directional doser connected to a tube (2 mm, inner diameter) that terminated 3 cm from the sample surface and 50 cm from the hot-cathode ionization gauge. IR data were accumulated by recording 256 scans with a resolution of 1 cm^{-1} at 110 K. Before each exposure, a spectrum of the clean sample was recorded as a background reference.

2.3. Catalytic Tests. The low-temperature WGS reaction over the Pt/TiO_2 catalysts was performed with a continuous-flow fixed-bed quartz tubular reactor (6 mm, inner diameter) under atmospheric pressure. 200 mg of sample (40−60 mesh) was placed between two layers of quartz wools inside the reactor, and pretreated by flowing a 20.0 vol % O_2/He mixture (30 mL min^{-1}) at 673 K for 1 h. After cooling down to 473 K under He follow (30 mL min^{-1}), the catalyst was exposed to the feed gas of 1.0 vol % CO/3.0 vol % H_2O/He (66.7 mL min^{-1}). The effluent from the reactor was analyzed online using gas chromatography equipped with a thermal conductivity detector and a flame ionization detector. To accurately determine the concentrations of CO and CO_2 in the outlet gases, a nickel catalyst converter, used for converting CO and CO_2 into methane, was placed before the flame ionization detector. Reaction rates were measured under differential reactor conditions with the CO conversion below 13% by adjusting the weight of catalyst and the flow rate of feed gas.

3. RESULTS AND DISCUSSION

3.1. PtO_x Clusters and Single-Atoms. Pt colloids of about 3 nm in size were deposited onto a rod-shaped brookite-TiO_2, forming the initial Pt/TiO_2 sample (Figures S1−S3). Air-calcination of this Pt/TiO_2 precursor at 773 K for 4 h yielded PtO_x clusters <1 nm on TiO_2 (the Pt−C sample), as evidenced by STEM (Figures 1A−C and S4). Most clusters

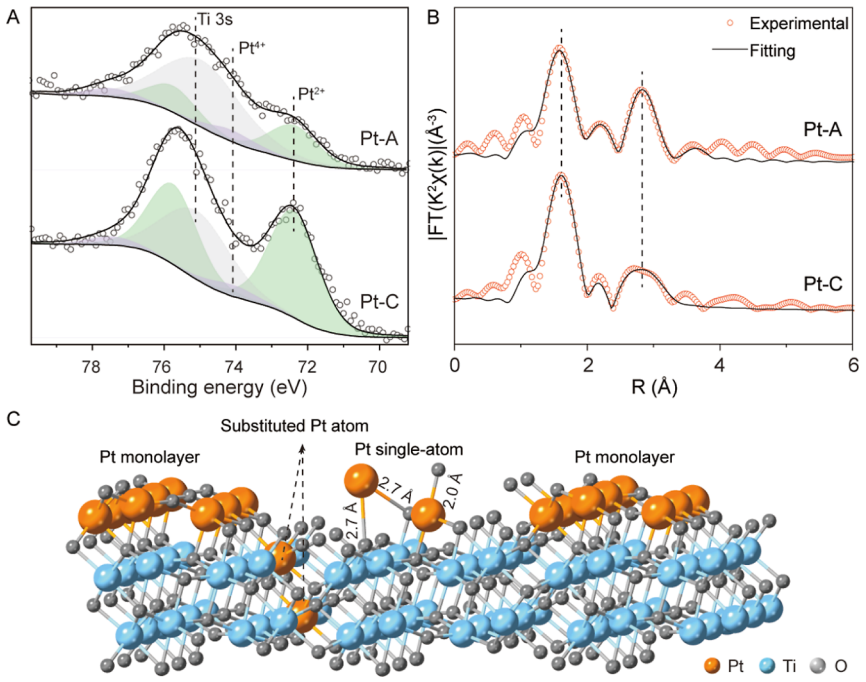

Figure 2. XPS spectra of Pt 4f (A) and Fourier transform of the k^2-weighted EXAFS spectra at the Pt L_3 edge (B) of the Pt−C and Pt−A samples. (C) Schematic illustration of the coordination environments of PtO_x monolayers and cationic Pt single-atoms over brookite TiO_2 {210}.

were less than 0.5 nm in a monolayer geometry, while few clusters had a relatively greater size of around 0.8 nm in a bilayer configuration. These ultrafine clusters consisted of loosely arranged Pt atoms anchored on the surface of TiO_2. In addition, an appreciable amount of Pt single-atoms was observed to locate around the clusters. When the Pt/TiO_2 precursor was subjected to a two-step air-calcination, i.e., first at 773 K for 24 h and then at 873 K for 10 h, the Pt particle decomposed into Pt single-atoms (the Pt−A sample, Figures 1D−F and S5). *Z*-contrast analysis on the STEM images revealed that a substantial amount of Pt single-atoms diffused into the subsurface/bulk of the TiO_2 support.[20,21] Meanwhile, few Pt dimers/trimers were seen occasionally, but the Pt atoms arranged randomly and loosely and thus could be viewed as single-atoms. These STEM results verified that the 3 nm Pt particle in the initial Pt/TiO_2 sample was oxidized and redispersed into mainly PtO_x monolayers on TiO_2 at 773 K. Upon calcination at 873 K, the monolayers further spitted into single-atoms that located on the surface and mostly in the subsurface/bulk of TiO_2. ICP analysis affirmed that Pt contents remained unchanged (0.19 wt %) in the samples before and after air-calcinations. This evidenced that the dispersion of the Pt particle into monolayers and single-atoms occurred via a solid−solid route, rather than the thermal evaporation process.[22−24]

XPS spectra of Pt 4f identified the chemical states of the surface Pt species in the Pt−C and Pt−A samples (Figure 2A). Deconvolution of the spectra yielded two types of Pt species. The spin−orbit doublet at 72.4/75.8 eV referred to Pt^{2+} species, while the doublet at 74.1/77.5 eV indicated Pt^{4+} species.[25,26] Of note, the binding energy at ∼75 eV included contributions from Ti 3s and Pt $4f_{5/2}$.[27−29] Quantitative analysis, by subtracting the contribution of Ti 3s, found that the Pt−C sample contained 90% Pt^{2+} and 10% Pt^{4+}, while the Pt−A sample consisted of 76% Pt^{2+} and 24% Pt^{4+}. This meant that increasing the temperature for air-calcination enhanced the fraction of Pt^{4+}. That is, the Pt single-atoms are presented as both Pt^{2+} and Pt^{4+} in different coordination environments in the Pt−A sample.

XANES spectra reaffirmed the PtO_x clusters and cationic Pt single-atoms in the two samples (Figure S6). The white line intensities at Pt L_3-edge located between Pt and PtO_2 foils, but were closer to that for PtO_2, characteristics for PtO_x.[30−32] Relative to the case of Pt−C, the white line decreased slightly in Pt−A, despite a higher content of Pt^{4+}. This might be caused by the second-nearest-neighboring Ti atoms that play a key role in redistributing electronic charge between Pt single-atom and TiO_2.[33] In other words, a change in the nearest-neighboring environment affects the electronic properties of Pt single-atoms. A similar phenomenon has been reported for $Pt/CeO_2−TiO_2$.[33] The XPS spectra revealed that the increase in Pt weight loading led to an increase in the fraction of Pt^{4+}. However, the XANES Pt L_3 edge white line weakened, which was ascribed to the influence from the nearby Ti atoms.

Fourier transformation in the *R*-space of the EXAFS spectra resolved the coordination environments of Pt atoms in the Pt−C and Pt−A samples (Figures 2B and S7). For having reasonable fitting models, four paths are involved: Pt−O_s, Pt−O_l, Pt−Pt, and Pt−Ti (Table S1). For the Pt−C sample, only the Pt−O_s path at a distance of 1.99 Å and with a coordination number (CN) of 4.9 was resolved, referring to Pt−O in PtO_x monolayers and/or Pt single-atoms in TiO_2 lattice.[34−38] The distinctly enlarged Pt−Pt distance (2.95 Å) with a CN of 1.5 suggested that Pt atoms coordinated via a bridging oxygen atom in PtO_x clusters.[34] In addition, a Pt−Ti path distanced at 3.11 Å with a CN of 3.0 was resolved, implicating that the Pt single-atoms were stabilized through ionic interaction with the lattice oxygen atoms in TiO_2.[21,36] These results are in line with the PtO_x monolayer geometry, as identified by STEM. For the Pt−A sample, besides the Pt−O_s (1.97 Å) path with a CN of 3.9, an additional Pt−O_l (2.73 Å) path with a CN of 4.3 was required to adequately account for the intensity between 2 and

3 Å. Such a longer Pt−O_l path has been applied to model the EXAFS data of oxide-supported Pt catalysts.[39−43] As STEM images in Figure 1 clearly evidenced the thermal decomposition of PtO_x clusters to Pt single-atoms, this Pt−O_l path referred to the loosely arranged Pt single-atoms over the TiO_2 surface.[42,43] Moreover, an additional Pt−Ti path at a distance of 3.56 Å with a CN of 2.8 was resolved in Pt−A. This significantly increased CN of Pt−Ti indicated that more Pt single-atoms diffused into subsurface/bulk TiO_2 in Pt−A, as observed by STEM. These results demonstrated that the Pt single-atoms presented in at least three types of coordination environments (Figure 2C). Some Pt atoms bonded to TiO_2 surface with a short Pt−O_s (1.97 Å) and elongated Pt−O_l (2.73 Å) bonds, while others diffused into the subsurface/bulk of TiO_2 (Pt−O_s, 1.97 Å; Pt−Ti, 3.11 and 3.56 Å). This is consistent with the Z-contrasts on the STEM images (Figure 1) and the coexistence of Pt^{2+} and Pt^{4+} in the XPS spectra (Figure 2A). Brookite TiO_2 has an orthorhombic structure with a unit cell at the space group *Pbca*.[44] The TiO_6 octahedra are distorted, and the oxygen atoms locate in two different positions. The six Ti−O bonds have different lengths, varying in the range 1.927−1.987 Å. This means that the CN of Ti−O is maximized to be 6 and its length varies in the lattice. The second nearest shell with a distance of seven Pt−Ti paths includes three Pt−Ti with a distance of 3.064 Å and four Pt−Ti at a distance of 3.5614 Å. Considering the bonding pattern (Pt−O−Ti) of Pt single-atoms in subsurface/bulk TiO_2, the maximum CN of the Pt−Ti path would be 7.0.

The dispersion of the Pt particle to PtO_x monolayers at 773 K and further to cationic Pt single-atoms at 873 K under oxidative atmosphere was intimately linked to the surface energy of the Pt particle and the surface property of brookite TiO_2.[34,45,46] The 3 nm Pt particle facilitated the oxidation of surface Pt atoms to form PtO_x species, while the {210} facets exposed by the rod-shaped brookite-TiO_2 provided sites to anchor the mobile PtO_x (Figure S2). The oxidation of surface atoms on the Pt particle to PtO_x lowered the cohesive energy of the metal particle and reduced the energy barrier for the detachment of Pt atoms, thus amplifying to break the Pt−Pt bond.[47−49] The {210} facets of brookite-TiO_2 are constructed by coordinatively unsaturated Ti5c and O2c atoms as well saturated Ti6c and O3c sites. The closely packed atomic configuration only along the [001] direction results in a higher surface energy (0.70 J m^{-2}).[44] Therefore, both unsaturated oxygen sites (O2c) and surface Ti sites could anchor the mobile PtO_x species.[47,50,51] In addition, some Pt single-atoms diffused into the subsurface or even the bulk of TiO_2, where the Pt atom substituted for a Ti atom and resided in a coordination-saturated environment, as evidenced by STEM, XPS, and EXAFS data.

The Pt/TiO_2 catalysts were tested for the low-temperature WGS reaction at 473 K. The conversion of CO was 23% over Pt−C but sharply declined to 3% on Pt−A (Figure 3), showing the superior performance of the Pt−C catalyst. For kinetic analysis, the reactions were performed by adjusting the conversion of CO at around 10% (Table S2), i.e., under a differential reactor condition. The specific reaction rate, based on Pt-mass, was 3.5×10^{-4} mol_{CO} g_{Pt}^{-1} s^{-1} on Pt−C but it dropped to 3.7×10^{-5} mol_{CO} g_{Pt}^{-1} s^{-1} over Pt−A. That is, the intrinsic activity of Pt−C was about one order of magnitude greater than that of Pt−A. Since the two samples had the same Pt content (0.19 wt %), this large difference in WGS activity implicated substantial changes in the size and spatial location

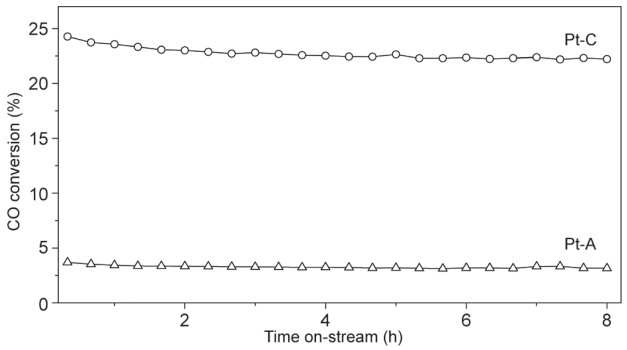

Figure 3. WGS reaction over the Pt−C and Pt−A catalysts. Reaction conditions: 473 K, 1.0 vol % CO/3.0 vol % H_2O/He, 20,000 mL g_{cat}^{-1} h^{-1}.

of Pt entities. As mentioned above, the Pt−C sample featured PtO_x monolayers over TiO_2, while the Pt−A sample consisted of cationic Pt single-atoms that mostly diffused into the subsurface/bulk of TiO_2 and thus became inaccessible for catalysis. The surface Pt species was tracked by FTIR spectroscopy using CO as a probe molecule at 110 K (Figure S8). The IR signal at about 2092 cm^{-1} observed for Pt−C was ascribed to CO bound to PtO_x species,[16,52−56] whereas nearly no CO signals over Pt−A were detected. This finding reaffirmed that most Pt single-atoms in Pt−A were buried into the subsurface/bulk of TiO_2 and thus were inaccessible for CO adsorption.[21] Overall, the Pt−C catalyst, containing mainly PtO_x monolayers, showed an appreciable WGS activity, but the Pt−A sample displayed a much lower activity simply because most cationic Pt single-atoms were located in the subsurface/bulk of TiO_2. With this regard, surface PtO_x clusters, for instance, in the form of Pt−O−Pt ensembles, on oxide-supports have been demonstrated to enhance CO oxidation activity, as compared to the surface Pt single-atoms.[52,57] A recent report showed that the onset of CO oxidation on Pt/CeO_2 was linked to the migration of cationic Pt single-sites to form small clusters containing few Pt atoms.[58] After breaking the Pt−O−Ce bond, Pt atoms moved across the oxide-support surface and aggregated into smaller PtO_x clusters, over which the reaction took place much faster than on the cationic Pt single-atoms.

To verify the structure change under WGS condition, the spent Pt−C catalyst was analyzed by XPS. Deconvolution of the Pt 4f XPS spectrum yielded two types of Pt species: 57% Pt^0 and 43% Pt^{2+} (Figure S9). As the fresh Pt−C sample contained 90% Pt^{2+} and 10% Pt^{4+}, this result evidenced that the PtO_x clusters were partially reduced during the WGS reaction. However, this did not alter the catalytic performance obviously because the reaction proceeded stably within 8 h. In other words, the electronic structure of PtO_x changed partially under WGS conditions at 473 K, but it did not cause appreciable variation in activity.

3.2. Metallic Pt Clusters. To tune the chemical state of the PtO_x clusters, the Pt−C sample was then subjected to H_2-reduction at 473−773 K, and the resulting samples were labeled as Pt−C-*T*, where *T* refers to the temperature. XRD patterns of the samples before and after H_2-reduction suggested the stable brookite phase of the TiO_2 support (Figure S10). The structural evolution of Pt entities was monitored by STEM, IR, and XPS. As the temperature was raised for H_2-treatment, PtO_x clusters were gradually reduced to metallic Pt clusters, and the geometric configuration was

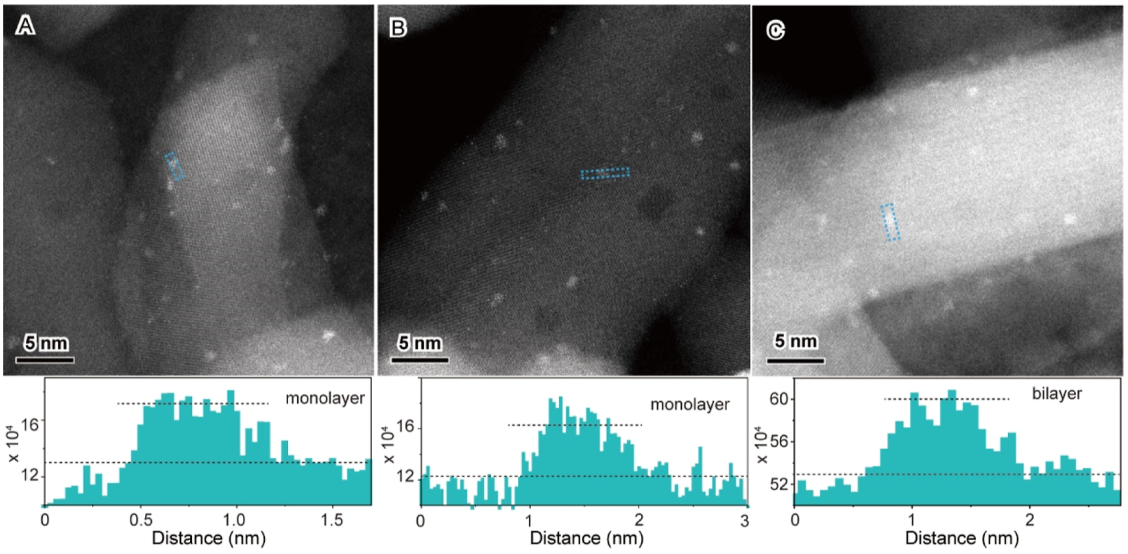

Figure 4. STEM images of the Pt−C-473 (A), Pt−C-573 (B), and Pt−C-773 (C) samples. The line intensity profiles correspond to the rectangular regions in the STEM images.

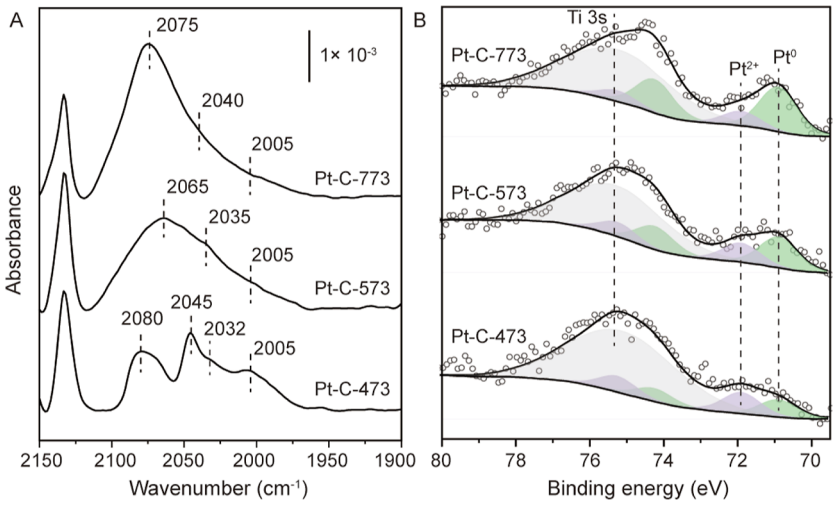

Figure 5. IR spectra of CO adsorption (A) and XPS spectra of Pt 4f (B) on the Pt−C-*T* samples.

shifted from monolayers to bilayers. Over the Pt−C-473 sample, Pt clusters ranged from 0.2 to 0.8 nm, with an average size of 0.6 nm in a monolayer geometry (Figures 4A and S11A−C). Few clusters had a relatively greater size of around 1.0 nm in a bilayer geometry. In addition, a substantial amount of loosely arranged Pt atoms are located around the Pt clusters. The corresponding CO-IR spectrum showed distinct bands at 2100−2000 cm^{-1} (Figure 5A), characteristics for CO linearly adsorbed on Pt sites.[59,60] As compared to the CO-IR spectrum of the Pt−C sample, where only a weak band at about 2092 cm^{-1} was observed (Figure S8), IR bands over the Pt−C-473 sample intensified apparently. The signal around 2080 cm^{-1} indicated that CO bound to cationic Pt single-atoms, while the low-lying bands at 2045, 2032, and 2005 cm^{-1} indicated CO adsorbed on smaller Pt clusters exposing mainly under-coordinated Pt sites.[16,61−63] This meant that Pt species enriched on the surface but presented at diverse coordination environments, resulting in a variety of CO-IR bands.[59] Nevertheless, Pt atoms with low-CNs are still predominantly present in the Pt−C-473 sample.

In the Pt−C-573 sample, Pt clusters enlarged slightly and the mean size was 0.8 nm, while the line intensity profiles indicated the coexistence of monolayers and bilayers (Figures 4B and S11D−F). This aggregation of Pt entities was further evidenced by the CO-IR band centered at 2065 cm^{-1} (Figure 5A), which was assigned to CO bound to Pt sites with higher CNs. In the case of the Pt−C-773 sample, Pt clusters averaged at 1.1 nm and had a bilayer geometry, while Pt single-atoms vanished completely (Figures 4C and S11G-I). The predominant IR band at 2075 cm^{-1} (Figure 5A), originating from CO adsorbed at highly coordinated Pt sites, supported this structural evolution. The chemical state of platinum in the Pt−C-*T* catalysts was investigated by XPS. Deconvolution of Pt 4f XPS spectra revealed the coexistence of Pt^0 and Pt^{2+} and the $Pt^0/(Pt^0 + Pt^{2+})$ ratio increased as raising the temperature for H_2-reduction (Figure 5B). For the Pt−C-473 sample, both Pt^0 and Pt^{2+} were detected with a $Pt^0/(Pt^0 + Pt^{2+})$ ratio of 0.45. The $Pt^0/(Pt^0 + Pt^{2+})$ ratio approached 0.75 for the Pt−C-773 sample. This is in line with the IR data that the predominant band, stemming from CO adsorption at the highly coordinated Pt sites, intensified remarkably. In

summary, STEM images, IR spectra, and XPS data collectively supported that the PtO_x monolayers in Pt−C reshaped into metallic Pt bilayers upon H_2-reduction at elevated temperatures along with the slight increase in size. In particular, the Pt−C-773 sample featured metallic Pt clusters of 1.1 nm in a bilayer geometry and at a $Pt^0/(Pt^0 + Pt^{2+})$ ratio of 0.75.

The Pt−C-*T* samples were then tested for the WGS reaction, and it was found interestingly that the activity increased with enlarging Pt clusters. The Pt−C-473 sample, containing Pt clusters averaged at 0.6 nm in a monolayer geometry, exhibited a CO conversion of 26% (Figure 6A). As

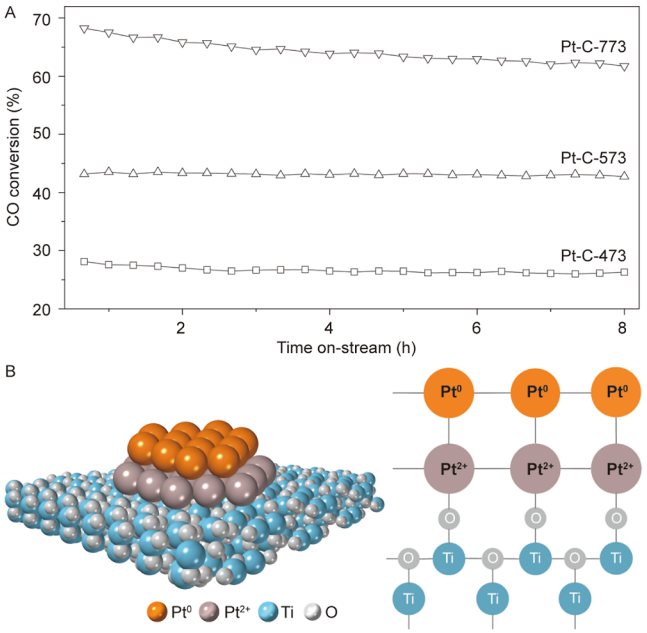

Figure 6. WGS reaction over the Pt−C-*T* catalysts (A) and schematic illustrations of the Pt bilayer geometry and the electronic characters of Pt atoms (B). Reaction conditions: 473 K, 1.0 vol % CO/3.0 vol % H_2O/He, 20,000 mL g_{cat}^{-1} h^{-1}.

Pt clusters were enlarged to 0.8−1.1 nm, the activity increased dramatically. The conversion of CO was 41% on Pt−C-573 and further increased to 62% over Pt−C-773. Kinetic measurements (Table S2), at a differential reactor condition, revealed that the specific reaction rate followed the order Pt−C-773 (6.8×10^{-4} mol_{CO} g_{Pt}^{-1} s^{-1}) > Pt−C-573 (4.3×10^{-4} mol_{CO} g_{Pt}^{-1} s^{-1}) > Pt−C-473 (3.8×10^{-4} mol_{CO} g_{Pt}^{-1} s^{-1}). All of these reaction data verified that the Pt−C-773 catalyst possessed a substantially enhanced activity, which should be related to the geometric and electronic structure of the metallic Pt bilayers.

Low-temperature WGS reaction occurs at the Pt−TiO_2 interfacial perimeter via a redox route: Pt adsorbs CO while TiO_2 surrounding the interface activates H_2O.[10] In this scenario, the coordination environment of the interfacial Pt atom is crucial for CO adsorption and activation. Based on the sizes and the geometries of Pt clusters in the above catalysts, the TOFs, in terms of interfacial Pt sites, were estimated (Table S2). The Pt−C and Pt−C-473 catalysts had practically identical TOFs (0.07−0.08 s^{-1}). Of note, the two samples had a similar Pt cluster size (0.5−0.6 nm) in a monolayer geometry but varied chemical state of Pt. The Pt−C sample consisted of 90% Pt^{2+} and 10% Pt^{4+}, while the Pt−C-473 sample consisted of 55% Pt^{2+} and 45% Pt^0. Moreover, the spent Pt−C sample contained 43% Pt^{2+} and 57% Pt^0, quite similar to the case in the Pt−C-473 sample. Considering their similar activities, it could be inferred that PtO_x clusters in Pt−C have been reduced partially by H_2 at 473 K and/or under the WGS conditions, but this variation in electronic property did not alter the activity essentially. CO-IR spectrum of the Pt−C-473 sample suggested that the Pt clusters exposed undercoordinated Pt sites at diverse coordination environments. The positively charged Pt atoms weakly adsorbed CO, as indicated by the characteristic signal around 2080 cm^{-1} and thus leading to a lower activity.[16,62] By contrast, the TOF increased sharply to 0.24 s^{-1} over the Pt−C-773 catalyst. As illustrated by STEM, IR, and XPS data, the metallic Pt bilayers had an average size of 1.1 nm. The interfacial Pt atoms were positively charged (Pt^{2+}) via interacting with TiO_2, while the surficial Pt atoms were metallic (Pt^0) and coordinated to the interfacial Pt^{2+} atoms (Figure 6B). This Pt−Pt bonding could modify the electronic character of the interfacial Pt site,[64−66] and consequently its interaction with CO.[10,65] Most likely, the Pt^0−Pt^{2+}−O−Ti configuration tuned the charge balance between surficial Pt^0 and interfacial Pt^{2+} for CO adsorption and activation in an appropriate manner, i.e., not too strong and not too weak, as evidenced by the characteristic IR band (2075 cm^{-1}) for CO adsorption on highly coordinated Pt sites (Figure 5A).

For comparison, a reference sample (Pt−P) was prepared by calcining the Pt/TiO_2 precursor at 673 K in air. The Pt particles had an average size of 3.3 nm and a hemisphere morphology with distinct interfaces with the TiO_2 support (Figure S12). When tested for the WGS reaction at 473 K, the specific reaction rate was 1.2×10^{-4} mol_{CO} g_{Pt}^{-1} s^{-1} (Table S2), much lower than that (3.8×10^{-4} mol_{CO} g_{Pt}^{-1} s^{-1}) of the Pt−C sample. The TOF, estimated by counting the number of interfacial Pt sites, however, was about 0.39 s^{-1}. This further evidenced the crucial role of the Pt−TiO_2 interface in the WGS reaction.

3.3. H_2-Reduction of Cationic Pt Single-Atoms. The Pt−A sample was also treated with H_2 at temperatures up to 773 K to reduce the number of cationic Pt single-atoms. The resulting samples were labeled as Pt−A-*T*, where T refers to the temperature. In the Pt−A-473 sample, STEM observations suggested that surface Pt atoms increased apparently (Figures 7A and S13A−C). This implicated the migration of Pt single-atoms from the subsurface or bulk to the surface of TiO_2. For the Pt−A-773 sample, Pt single-atoms still dominated, while Pt clusters of about 1 nm were seen occasionally (Figures 7B and S13D−F). The appearance of Pt clusters was further evidenced by XAS. The white line intensities of Pt−A-473 and Pt−A-773 located between PtO_2 and Pt foils (Figure 7C), indicating a mixture of Pt^0 and Pt^{2+}/Pt^{4+}. The reduced intensity in the Pt−A-773 sample implicated an increased percentage of metallic Pt.[30−32] Pt−O path in the EXAFS spectra weakened, but that of the Pt−Pt path, characteristics for metallic Pt clusters, intensified apparently (Figure 7D). CO-IR spectra evidenced the reduction and aggregation of Pt single-atoms. The Pt−A-473 sample showed very weak and broad bands at 2100−2000 cm^{-1} (Figure 7E), stemming from the adsorption of CO on Pt in diverse coordination environments. This result verified that, compared to the inaccessible Pt sites on the Pt−A sample, Pt atoms migrated from the subsurface/bulk to the surface of TiO_2. The Pt−A-773 sample showed distinctive bands for CO adsorption on the Pt sites. The signal at 2099 cm^{-1} was ascribed to CO adsorption at cationic Pt single-atoms, while

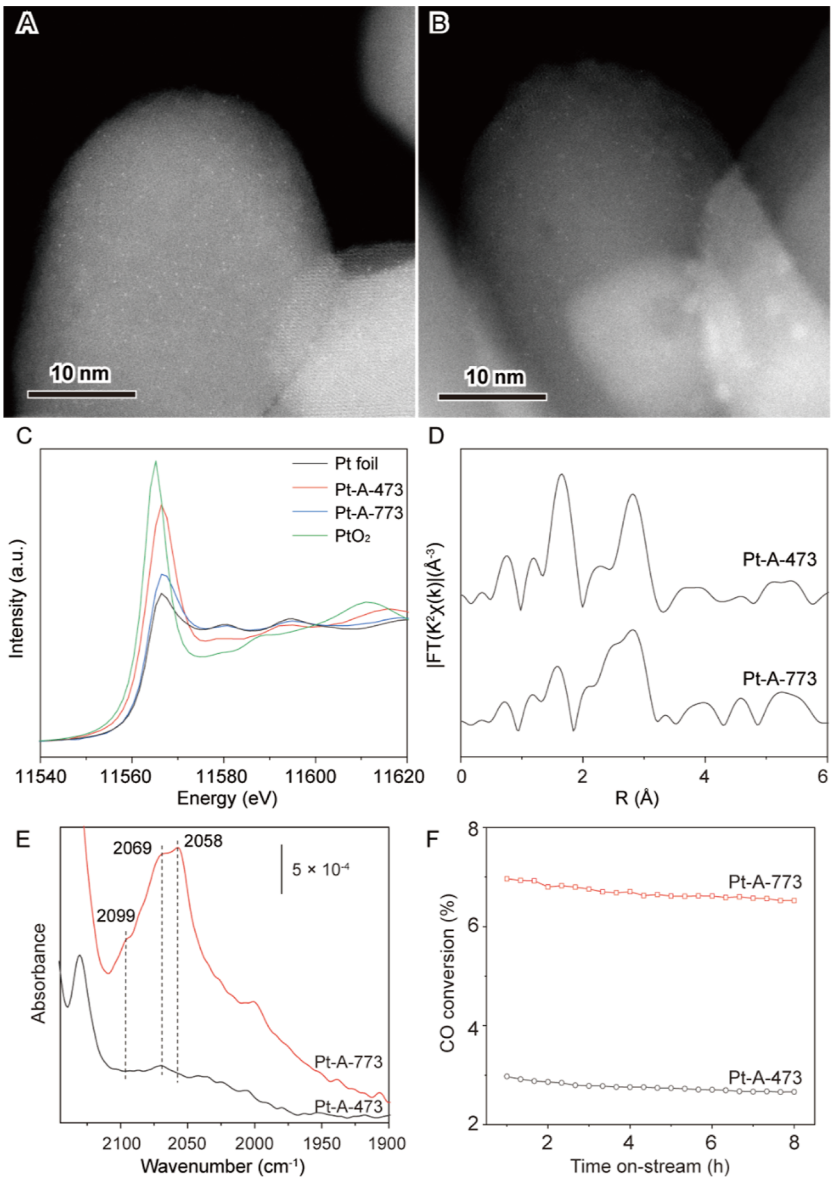

Figure 7. Structure and catalytic performance of the Pt−A-473 and Pt−A-773 samples. (A,B) STEM images; (C,D) XANES and Fourier transform of the k^2-weighted EXAFS spectra at Pt L_3 edge; (E) CO-IR spectra; and (F) CO conversions. Reaction conditions: 473 K, 1 vol % CO/3 vol % H_2O/He, 20,000 mL g_{cat}^{-1} h^{-1}.

the intense bands at 2069 and 2058 cm^{-1} indicated CO bound to Pt sites of ultrafine Pt clusters.[54,55] These STEM, EXAFS, and IR data collectively illustrated that some Pt single-atoms, originally located at the subsurface/bulk of TiO_2, migrated and combined into tiny clusters over the TiO_2 surface. When tested for the low-temperature WGS reaction, the Pt−A-473 catalyst showed a similar performance to the Pt−A sample, with a CO conversion of around 3%. Over the Pt−A-773 catalyst, however, the conversion of CO increased to 7% (Figure 7F), evidencing that Pt clusters, even if minority, largely contributed to the activity.

4. CONCLUSIONS

Upon air calcination, 3 nm Pt particles supported by a rod-shaped brookite-TiO_2 dispersed into subnanometric PtO_x clusters at 773 K and cationic Pt single-atoms at 873 K. The PtO_x clusters averaged at 0.5 nm in size and presented mainly in a monolayer geometry, while the cationic Pt single-atoms not only located on the surface of TiO_2 but also diffused into the subsurface/bulk of TiO_2, existing in diverse coordination environments. The PtO_x monolayers were more active for the low-temperature WGS reaction than for the cationic Pt single-atoms that were mostly inaccessible for catalysis. More importantly, the subsequent H_2-reduction of PtO_x monolayers at 773 K yielded metallic Pt clusters that enhanced the WGS activity significantly. The metallic Pt clusters had a mean size of 1.1 nm in a bilayer geometry at a $Pt^0/(Pt^0 + Pt^{2+})$ ratio of 0.75, where the surficial metallic Pt^0 atoms tuned the electronic property of the positively charged interfacial Pt^{2+} atoms, thereby facilitating CO adsorption and activation.

AUTHOR INFORMATION

Corresponding Authors

Yong Li − *State Key Laboratory of Catalysis, Chinese Academy of Sciences, Dalian Institute of Chemical Physics, Dalian 116023, China;* orcid.org/0000-0003-4830-9210; Email: yongli@dicp.ac.cn

Yuemin Wang − *Institute of Functional Interfaces, Karlsruhe Institute of Technology, Eggenstein-Leopoldshafen 76344, Germany;* orcid.org/0000-0002-9963-5473; Email: yuemin.wang@kit.edu

Wenjie Shen − *State Key Laboratory of Catalysis, Chinese Academy of Sciences, Dalian Institute of Chemical Physics, Dalian 116023, China;* orcid.org/0000-0002-3071-9556; Email: shen98@dicp.ac.cn

Authors

Wenning Zhao − *State Key Laboratory of Catalysis, Chinese Academy of Sciences, Dalian Institute of Chemical Physics, Dalian 116023, China*

Junjun Wang − *Engineering Research Center of Environmental Materials and Membrane Technology of Hubei Province, School of Materials Science and Engineering, Wuhan Institute of Technology, Wuhan 430074, China; Institute of Functional Interfaces, Karlsruhe Institute of Technology, Eggenstein-Leopoldshafen 76344, Germany*

Xixiong Zhang − *State Key Laboratory of Catalysis, Chinese Academy of Sciences, Dalian Institute of Chemical Physics, Dalian 116023, China*

Guanghui Zhang − *State Key Laboratory of Fine Chemicals, Frontier Science Center for Smart Materials, PSU-DUT Joint Center for Energy Research, School of Chemical Engineering, Dalian University of Technology, Dalian 116024, China;* orcid.org/0000-0002-5854-6909

Zheng Jiang − *National Synchrotron Radiation Laboratory, University of Science and Technology of China, Hefei 230026, China;* orcid.org/0000-0003-4297-464X

Mingrun Li − *State Key Laboratory of Catalysis, Chinese Academy of Sciences, Dalian Institute of Chemical Physics, Dalian 116023, China*

Yan Zhou − *State Key Laboratory of Catalysis, Chinese Academy of Sciences, Dalian Institute of Chemical Physics, Dalian 116023, China;* orcid.org/0000-0002-9847-0806

Author Contributions

[#]W.Z., J.W., and X.Z. contributed equally to the work.

Notes

The authors declare no competing financial interest.

■ ACKNOWLEDGMENTS

This work was supported by the National Key R&D Program of China (2021YFA1502802), the Deutsche Forschungsgemeinschaft (DFG, German Research Foundation—project-ID 426888090—SFB 1441), and the National Natural Science Foundation of China (22002164).

■ REFERENCES

(1) Liu, L.; Corma, A. Metal catalysts for heterogeneous catalysis: from single atoms to nanoclusters and nanoparticles. *Chem. Rev.* **2018**, *118*, 4981−5079.

(2) Beniya, A.; Higashi, S. Towards dense single-atom catalysts for future automotive applications. *Nat. Catal.* **2019**, *2*, 590−602.

(3) Farrauto, R. J.; Deeba, M.; Alerasool, S. Gasoline automobile catalysis and its historical journey to cleaner air. *Nat. Catal.* **2019**, *2*, 603−613.

(4) Zhang, L.; Zhou, M.; Wang, A.; Zhang, T. Selective hydrogenation over supported metal catalysts: from nanoparticles to single atoms. *Chem. Rev.* **2020**, *120*, 683−733.

(5) Li, L.; Chang, X.; Lin, X.; Zhao, Z. J.; Gong, J. Theoretical insights into single-atom catalysts. *Chem. Soc. Rev.* **2020**, *49*, 8156−8178.

(6) Li, Z.; Ji, S.; Liu, Y.; Cao, X.; Tian, S.; Chen, Y.; Niu, Z.; Li, Y. Well-defined materials for heterogeneous catalysis: from nanoparticles to isolated single-atom sites. *Chem. Rev.* **2020**, *120*, 623−682.

(7) Guo, Y.; Wang, M.; Zhu, Q.; Xiao, D.; Ma, D. Ensemble effect for single-atom, small cluster and nanoparticle catalysts. *Nat. Catal.* **2022**, *5*, 766−776.

(8) Kaiser, S. K.; Chen, Z.; Faust Akl, D.; Mitchell, S.; Pérez-Ramírez, J. Single-atom catalysts across the periodic table. *Chem. Rev.* **2020**, *120*, 11703−11809.

(9) Giulimondi, V.; Mitchell, S.; Pérez-Ramírez, J. Challenges and opportunities in engineering the electronic structure of single-atom catalysts. *ACS Catal.* **2023**, *13*, 2981−2997.

(10) Ammal, S. C.; Heyden, A. Understanding the nature and activity of supported platinum catalysts for the water−gas shift reaction: from metallic nanoclusters to alkali-stabilized single-atom cations. *ACS Catal.* **2019**, *9*, 7721−7740.

(11) Chen, Y.; Lin, J.; Wang, X. Noble-metal based single-atom catalysts for the water-gas shift reaction. *Chem. Commun.* **2022**, *58*, 208−222.

(12) Zhou, L.; Liu, Y.; Liu, S.; Zhang, H.; Wu, X.; Shen, R.; Liu, T.; Gao, J.; Sun, K.; Li, B.; Jiang, J. For more and purer hydrogen-the progress and challenges in water gas shift reaction. *J. Energy Chem.* **2023**, *83*, 363−396.

(13) Panagiotopoulou, P.; Kondarides, D. I. Effect of morphological characteristics of TiO_2-supported noble metal catalysts on their activity for the water-gas shift reaction. *J. Catal.* **2004**, *225*, 327−336.

(14) Iida, H.; Kondo, K.; Igarashi, A. Effect of Pt precursors on catalytic activity of Pt/TiO_2 (rutile) for water gas shift reaction at low-temperature. *Catal. Commun.* **2006**, *7*, 240−244.

(15) Zhao, H.; Yao, S.; Zhang, M.; Huang, F.; Fan, Q.; Zhang, S.; Liu, H.; Ma, D.; Gao, C. Ultra-small platinum nanoparticles encapsulated in sub-50 nm hollow titania nanospheres for low-temperature water-gas shift reaction. *ACS Appl. Mater. Interfaces* **2018**, *10*, 36954−36960.

(16) DeRita, L.; Dai, S.; Lopez-Zepeda, K.; Pham, N.; Graham, G. W.; Pan, X.; Christopher, P. Catalyst architecture for stable single atom dispersion enables site-specific spectroscopic and reactivity measurements of CO adsorbed to Pt atoms, oxidized Pt clusters, and metallic Pt clusters on TiO_2. *J. Am. Chem. Soc.* **2017**, *139*, 14150−14165.

(17) Ding, K.; Gulec, A.; Johnson, A. M.; Schweitzer, N. M.; Stucky, G. D.; Marks, L. D.; Stair, P. C. Identification of active sites in CO

oxidation and water-gas shift over supported Pt catalysts. *Science* **2015**, *350*, 189−192.
(18) Yang, M.; Liu, J.; Lee, S.; Zugic, B.; Huang, J.; Allard, L. F.; Flytzani-Stephanopoulos, M. A common single-site Pt(II)−O(OH)$_x$− species stabilized by sodium on "active" and "inert" supports catalyzes the water-gas shift reaction. *J. Am. Chem. Soc.* **2015**, *137*, 3470−3473.
(19) Roldan Cuenya, B.; Behafarid, F. Nanocatalysis: size- and shape-dependent chemisorption and catalytic reactivity. *Surf. Sci. Rep.* **2015**, *70*, 135−187.
(20) Chang, T. Y.; Tanaka, Y.; Ishikawa, R.; Toyoura, K.; Matsunaga, K.; Ikuhara, Y.; Shibata, N. Direct imaging of Pt single atoms adsorbed on TiO_2 (110) surfaces. *Nano Lett.* **2014**, *14*, 134−138.
(21) Chen, L.; Unocic, R. R.; Hoffman, A. S.; Hong, J.; Braga, A. H.; Bao, Z.; Bare, S. R.; Szanyi, J. Unlocking the catalytic potential of TiO_2-supported Pt single atoms for the reverse water-gas shift reaction by altering their chemical environment. *JACS Au* **2021**, *1*, 977−986.
(22) Jones, J.; Xiong, H.; DeLaRiva, A. T.; Peterson, E. J.; Pham, H.; Challa, S. R.; Qi, G.; Oh, S.; Wiebenga, M. H.; Pereira Hernández, X. I.; Wang, Y.; Datye, A. K. Thermally stable single-atom platinum-on-ceria catalysts via atom trapping. *Science* **2016**, *353*, 150−154.
(23) Oh, J.; Beck, A.; Goodman, E. D.; Roling, L. T.; Boucly, A.; Artiglia, L.; Abild-Pedersen, F.; van Bokhoven, J. A.; Cargnello, M. Colloidally engineered Pd and Pt catalysts distinguish surface- and vapor-mediated deactivation mechanisms. *ACS Catal.* **2023**, *13*, 1812−1822.
(24) Beck, A.; Frey, H.; Huang, X.; Clark, A. H.; Goodman, E. D.; Cargnello, M.; Willinger, M.; van Bokhoven, J. A. Controlling the strong metal-support interaction overlayer structure in Pt/TiO_2 catalysts prevents particle evaporation. *Angew. Chem., Int. Ed.* **2023**, *62*, No. e202301468.
(25) Macino, M.; Barnes, A. J.; Althahban, S. M.; Qu, R.; Gibson, E. K.; Morgan, D. J.; Freakley, S. J.; Dimitratos, N.; Kiely, C. J.; Gao, X.; Beale, A. M.; Bethell, D.; He, Q.; Sankar, M.; et al. Tuning of catalytic sites in Pt/TiO_2 catalysts for the chemoselective hydrogenation of 3-nitrostyrene. *Nat. Catal.* **2019**, *2*, 873−881.
(26) Frey, H.; Beck, A.; Huang, X.; van Bokhoven, J. A.; Willinger, M. G. Dynamic interplay between metal nanoparticles and oxide support under redox conditions. *Science* **2022**, *376*, 982−987.
(27) Kuo, C.-T.; Lu, Y.; Kovarik, L.; Engelhard, M.; Karim, A. M. Structure sensitivity of acetylene semi-hydrogenation on Pt single atoms and subnanometer clusters. *ACS Catal.* **2019**, *9*, 11030−11041.
(28) Petzoldt, P.; Eder, M.; Mackewicz, S.; Blum, M.; Kratky, T.; Günther, S.; Tschurl, M.; Heiz, U.; Lechner, B. A. J. Tuning strong metal−support interaction kinetics on Pt-loaded TiO_2(110) by choosing the pressure: a combined ultrahigh vacuum/near-ambient pressure XPS study. *J. Phys. Chem. C* **2022**, *126*, 16127−16139.
(29) Chen, M.; Wang, W.; Qiu, Y.; Wen, H.; Li, G.; Yang, Z.; Wang, P. Identification of active sites in HCHO oxidation over TiO_2-supported Pt catalysts. *ACS Catal.* **2022**, *12*, 5565−5573.
(30) Pazmiño, J. H.; Shekhar, M.; Damion Williams, W.; Cem Akatay, M.; Miller, J. T.; Nicholas Delgass, W.; Ribeiro, F. H. Metallic Pt as active sites for the water-gas shift reaction on alkali-promoted supported catalysts. *J. Catal.* **2012**, *286*, 279−286.
(31) Han, B.; Guo, Y.; Huang, Y.; Xi, W.; Xu, J.; Luo, J.; Qi, H.; Ren, Y.; Liu, X.; Qiao, B.; Zhang, T. Strong metal-support interactions between Pt single atoms and TiO_2. *Angew. Chem., Int. Ed.* **2020**, *59*, 11824−11829.
(32) Li, Y.; Kottwitz, M.; Vincent, J. L.; Enright, M. J.; Liu, Z.; Zhang, L.; Huang, J.; Senanayake, S. D.; Yang, W.-C. D.; Crozier, P. A.; Nuzzo, R. G.; Frenkel, A. I. Dynamic structure of active sites in ceria-supported Pt catalysts for the water gas shift reaction. *Nat. Commun.* **2021**, *12*, 914.
(33) Wang, H.; Rui, N.; Senanayake, S. D.; Zhang, L.; Li, Y.; Frenkel, A. I. Tuning the placement of Pt "single atoms" on a mixed CeO_2-TiO_2 support. *J. Phys. Chem. C* **2022**, *126*, 16187−16193.
(34) Nur, A. S. M.; Funada, E.; Kiritoshi, S.; Matsumoto, A.; Kakei, R.; Hinokuma, S.; Yoshida, H.; Machida, M. Phase-dependent formation of coherent interface structure between PtO_2 and TiO_2 and its impact on thermal decomposition behavior. *J. Phys. Chem.C* **2018**, *122*, 662−669.
(35) Chen, Y.; Ji, S.; Sun, W.; Chen, W.; Dong, J.; Wen, J.; Zhang, J.; Li, Z.; Zheng, L.; Chen, C.; Peng, Q.; Wang, D.; Li, Y. Discovering partially charged single-atom Pt for enhanced anti-markovnikov alkene hydrosilylation. *J. Am. Chem. Soc.* **2018**, *140*, 7407−7410.
(36) DeRita, L.; Resasco, J.; Dai, S.; Boubnov, A.; Thang, H. V.; Hoffman, A. S.; Ro, I.; Graham, G. W.; Bare, S. R.; Pacchioni, G.; Pan, X.; Christopher, P. Structural evolution of atomically dispersed Pt catalysts dictates reactivity. *Nat. Mater.* **2019**, *18*, 746−751.
(37) Chen, Y.; Ji, S.; Sun, W.; Lei, Y.; Wang, Q.; Li, A.; Chen, W.; Zhou, G.; Zhang, Z.; Wang, Y.; Zheng, L.; Zhang, Q.; Gu, L.; Han, X.; Wang, D.; Li, Y. Engineering the atomic interface with single platinum atoms for enhanced photocatalytic hydrogen production. *Angew. Chem., Int. Ed.* **2020**, *59*, 1295−1301.
(38) Piccolo, L.; Afanasiev, P.; Morfin, F.; Len, T.; Dessal, C.; Rousset, J. L.; Aouine, M.; Bourgain, F.; Aguilar-Tapia, A.; Proux, O.; Chen, Y.; Soler, L.; Llorca, J. Operando X-ray absorption spectroscopy investigation of photocatalytic hydrogen evolution over ultradispersed Pt/TiO_2 catalysts. *ACS Catal.* **2020**, *10*, 12696−12705.
(39) Alexeev, O. S.; Chin, S. Y.; Engelhard, M. H.; Ortiz-Soto, L.; Amiridis, M. D. Effects of reduction temperature and metal-support interactions on the catalytic activity of Pt/γ-Al_2O_3 and Pt/TiO_2 for the oxidation of CO in the presence and absence of H_2. *J. Phys. Chem. B* **2005**, *109*, 23430−23443.
(40) Ahmadi, M.; Timoshenko, J.; Behafarid, F.; Roldan Cuenya, B. Tuning the structure of Pt nanoparticles through support interactions: an in situ polarized X-ray absorption study coupled with atomistic simulations. *J. Phys. Chem. C* **2019**, *123*, 10666−10676.
(41) Siani, A.; Alexeev, O. S.; Lafaye, G.; Amiridis, M. D. The effect of Fe on SiO_2-supported Pt catalysts: structure, chemisorptive, and catalytic properties. *J. Catal.* **2009**, *266*, 26−38.
(42) Cheng, X.; Li, Y.; Zheng, L.; Yan, Y.; Zhang, Y.; Chen, G.; Sun, S.; Zhang, J. Highly active, stable oxidized platinum clusters as electrocatalysts for the hydrogen evolution reaction. *Energy Environ. Sci.* **2017**, *10*, 2450−2458.
(43) Zhu, Y.; Luo, Y.; Yao, J.; Dai, W.; Zhong, X.; Lu, T.; Pan, Y. Atomically dispersed Pt-O coordination boosts highly active and durable acidic hydrogen evolution reaction. *Chem. Eng. J.* **2022**, *440*, 135957.
(44) Gong, X.-Q.; Selloni, A. First-principles study of the structures and energetics of stoichiometric brookite TiO_2 surfaces. *Phys. Rev. B* **2007**, *76*, 235307.
(45) Tabib Zadeh Adibi, P.; Pingel, T.; Olsson, E.; Grönbeck, H.; Langhammer, C. Pt nanoparticle sintering and redispersion on a heterogeneous nanostructured support. *J. Phys. Chem.C* **2016**, *120*, 14918−14925.
(46) Wan, Q.; Hu, S.; Dai, J.; Chen, C.; Li, W.-X. First-principles kinetic study for Ostwald ripening of late transition metals on TiO_2(110). *J. Phys. Chem. C* **2019**, *123*, 1160−1169.
(47) Zhou, Y.; Muhich, C. L.; Neltner, B. T.; Weimer, A. W.; Musgrave, C. B. Growth of Pt particles on the anatase TiO_2 (101) surface. *J. Phys. Chem. C* **2012**, *116*, 12114−12123.
(48) Plessow, P. N.; Abild-Pedersen, F. Sintering of Pt nanoparticles via volatile PtO_2: simulation and comparison with experiments. *ACS Catal.* **2016**, *6*, 7098−7108.
(49) Wang, X.; van Bokhoven, J. A.; Palagin, D. Ostwald ripening versus single atom trapping: towards understanding platinum particle sintering. *Phys. Chem. Chem. Phys.* **2017**, *19*, 30513−30519.
(50) Han, Y.; Liu, C. J.; Ge, Q. Interaction of Pt clusters with the anatase TiO_2(101) surface: a first principles study. *J. Phys. Chem. B* **2006**, *110*, 7463−7472.
(51) Gong, X. Q.; Selloni, A.; Dulub, O.; Jacobson, P.; Diebold, U. Small Au and Pt clusters at the anatase TiO_2(101) surface: behavior at terraces, steps, and surface oxygen vacancies. *J. Am. Chem. Soc.* **2008**, *130*, 370−381.
(52) Wang, H.; Liu, J.-X.; Allard, L. F.; Lee, S.; Liu, J.; Li, H.; Wang, J.; Wang, J.; Oh, S. H.; Li, W.; Flytzani-Stephanopoulos, M.; Shen, M.;

Goldsmith, B. R.; Yang, M. Surpassing the single-atom catalytic activity limit through paired Pt-O-Pt ensemble built from isolated Pt_1 atoms. *Nat. Commun.* **2019**, *10*, 3808.
(53) Kottwitz, M.; Li, Y.; Palomino, R. M.; Liu, Z.; Wang, G.; Wu, Q.; Huang, J.; Timoshenko, J.; Senanayake, S. D.; Balasubramanian, M.; Lu, D.; Nuzzo, R. G.; Frenkel, A. I. Local structure and electronic state of atomically dispersed Pt supported on nanosized CeO_2. *ACS Catal.* **2019**, *9*, 8738−8748.
(54) Jiang, D.; Yao, Y.; Li, T.; Wan, G.; Pereira-Hernández, X. I.; Lu, Y.; Tian, J.; Khivantsev, K.; Engelhard, M. H.; Sun, C.; García-Vargas, C. E.; Hoffman, A. S.; Bare, S. R.; Datye, A. K.; Hu, L.; Wang, Y. Tailoring the local environment of platinum in single-atom Pt_1/CeO_2 catalysts for robust low-temperature CO oxidation. *Angew. Chem., Int. Ed.* **2021**, *60*, 26054−26062.
(55) Zhang, Z.; Tian, J.; Lu, Y.; Yang, S.; Jiang, D.; Huang, W.; Li, Y.; Hong, J.; Hoffman, A. S.; Bare, S. R.; Engelhard, M. H.; Datye, A. K.; Wang, Y. Memory-dictated dynamics of single-atom Pt on CeO_2 for CO oxidation. *Nat. Commun.* **2023**, *14*, 2664.
(56) Wang, P.; Liu, G.; Hao, Z.; Zhang, H.; Li, Y.; Sun, W.; Zheng, L.; Zhan, S. In situ formation of cocatalytic sites boosts single-atom catalysts for nitrogen oxide reduction. *Proc. Natl. Acad. Sci. U.S.A.* **2023**, *120*, No. e2216584120.
(57) Dessal, C.; Len, T.; Morfin, F.; Rousset, J.-L.; Aouine, M.; Afanasiev, P.; Piccolo, L. Dynamics of single Pt atoms on alumina during CO oxidation monitored by operando X-ray and infrared spectroscopies. *ACS Catal.* **2019**, *9*, 5752−5759.
(58) Maurer, F.; Jelic, J.; Wang, J.; Gänzler, A.; Dolcet, P.; Wöll, C.; Wang, Y.; Studt, F.; Casapu, M.; Grunwaldt, J. D. Tracking the formation, fate and consequence for catalytic activity of Pt single sites on CeO_2. *Nat. Catal.* **2020**, *3*, 824−833.
(59) Avanesian, T.; Dai, S.; Kale, M. J.; Graham, G. W.; Pan, X.; Christopher, P. Quantitative and atomic-scale view of CO-induced Pt nanoparticle surface reconstruction at saturation coverage via DFT calculations coupled with in situ TEM and IR. *J. Am. Chem. Soc.* **2017**, *139*, 4551−4558.
(60) Ren, X.; Gobrogge, E. A.; Lundgren, C. A. Titrating Pt surface with CO molecules. *J. Phys. Chem. Lett.* **2019**, *10*, 6306−6315.
(61) Kappers, M. J.; van der Maas, J. H. Correlation between CO frequency and Pt coordination number. A DRIFT study on supported Pt catalysts. *Catal. Lett.* **1991**, *10*, 365−373.
(62) Aleksandrov, H. A.; Neyman, K. M.; Hadjiivanov, K. I.; Vayssilov, G. N. Can the state of platinum species be unambiguously determined by the stretching frequency of an adsorbed CO probe molecule? *Phys. Chem. Chem. Phys.* **2016**, *18*, 22108−22121.
(63) Tigwell, M.; Douthwaite, M.; Smith, L. R.; Dummer, N. F.; Morgan, D. J.; Bethell, D.; Taylor, S. H.; Hutchings, G. J. Investigating catalytic properties which influence dehydration and oxidative dehydrogenation in aerobic glycerol oxidation over Pt/TiO_2. *J. Phys. Chem. C* **2022**, *126*, 15651−15661.
(64) Lykhach, Y.; Kozlov, S. M.; Skála, T.; Tovt, A.; Stetsovych, V.; Tsud, N.; Dvořák, F.; Johánek, V.; Neitzel, A.; Mysliveček, J.; Fabris, S.; Matolín, V.; Neyman, K. M.; Libuda, J. Counting electrons on supported nanoparticles. *Nat. Mater.* **2016**, *15*, 284−288.
(65) Ellaby, T.; Briquet, L.; Sarwar, M.; Thompsett, D.; Skylaris, C. K. Modification of O and CO binding on Pt nanoparticles due to electronic and structural effects of titania supports. *J. Chem. Phys.* **2019**, *151*, 114702.
(66) Beniya, A.; Higashi, S.; Ohba, N.; Jinnouchi, R.; Hirata, H.; Watanabe, Y. CO oxidation activity of non-reducible oxide-supported mass-selected few-atom Pt single-clusters. *Nat. Commun.* **2020**, *11*, 1888.